

[¹⁸F]-labeled positron emission tomography ligand for the histamine H4 receptor

Agnieszka Zak¹ | Lucas Lemaire¹ | Sylvie Chalon²  | Gabrielle Chicheri^{2,3} |
Hamid Marzag¹ | Sylvie Bodard² | Sophie Sérrière² | Sylvain Routier¹  |
Frédéric Buron¹  | Johnny Vercouillie^{2,3,4} 

¹Institut de Chimie Organique et Analytique, Université d'Orléans, UMR CNRS 7311, Orléans, France

²UMR 1253, iBrain, Université de Tours, Inserm, Tours, France

³CERRP, Université de Tours, Tours, France

⁴INSERM CIC 1415, University Hospital, Tours, France

Correspondence

Johnny Vercouillie, UMR 1253, iBrain, Université de Tours, Inserm, Tours, France.

Email: vercouillie@univ-tours.fr

Funding information

Agence Nationale de la Recherche, Grant/Award Number: Labex IRON, ANR11-LABX-0018-01; FP7 Health, Grant/Award Number: INMIND

We synthesized 5-[¹⁸F]-fluoro-1*H*-indol-2-yl)(4-methyl-1-piperazinyl)methanone ([¹⁸F]5) via a Suzuki approach starting from a protected pinacol borane precursor followed by acidic hydrolysis of the *t*-Boc protecting group. The non-optimized radiochemical yield was $5.7 \pm 1.35\%$, radiochemical purity was over 99%, and molar activity was 100.7 ± 34.5 GBq/ μmol ($n = 3$). [¹⁸F]5 was stable in rat plasma for at least 4 h and was evaluated by μPET imaging and biodistribution using a unilateral quinolinic acid rat model of neuroinflammation. The time-activity curve showed that [¹⁸F]5 entered the brain immediately after intravenous injection and then left it progressively with a very low level reached from 30 min after injection. The biodistribution study showed no difference in the accumulation of [¹⁸F]5 between the lesioned and intact side of the brain and between control rats and animals pretreated with a saturating dose of JNJ-777120 as a specific H4R antagonist. Hence, despite its *in vitro* nanomolar affinity for H4R, and its ability to cross the blood–brain barrier in rats, [¹⁸F]5 does not appear suitable to image *in vivo* the receptor by PET.

KEYWORDS

¹⁸F PET, agonism, H4 receptor, indole, radiolabeling

1 | INTRODUCTION

Histamine (2-[1*H*-imidazol-4-yl]ethanamine) is an endogenous short-acting biogenic amine implicated in various physiological and pathophysiological processes. Besides its peripheral functions, it plays an important role in the central nervous system (CNS) as a neurotransmitter and immunomodulator, with various functions in different circuitries. Histamine exerts its effects primarily by binding to four G protein-coupled receptor (GPCR) subtypes: H1R, H2R, H3R, and H4R.¹ Based on results obtained in the different histamine receptor subtypes of knockout mice models, it appeared that both H1R and H2R are

expressed ubiquitously and have a role in inflammation and allergy.¹ Moreover, H3Rs are mainly localized on the histaminergic neuron endings. These receptors are able to affect behavior.² Concerning the later discovered subtype H4, its precise localization and role are still poorly elucidated.^{2,3} However, data showed that H4R has a strong implication in the regulation of *in vivo* microglial activation by histamine.⁴ In addition, the H4R antagonist and partial agonist⁵ JNJ-777120 were recently shown to inhibit the pro-inflammatory M1 phenotype of microglia in a lesion-induced rat model of Parkinson's disease (PD), with beneficial effects on the survival and functioning of dopaminergic neurons.⁶

There is increasing evidence that inflammation plays a crucial role in PD as in other neurodegenerative diseases, in particular through microglia activation.⁷ In this context, the imaging of neurionflammation by positron emission tomography (PET) is now a highly relevant tool in a number of brain disorders, and the main molecular target explored to date for this aim is the 18-kDa translocator protein (TSPO) overexpressed in activated microglia.⁸ However, in view of several limitations with brain TSPO PET exploration, alternative and/or complementary molecular targets are currently being actively searched for.⁹ Among these potential new targets, H4R appears as a promising candidate.

To date, two carbon-11-labeled analogs (Figure 1) of the highly potent and subtype-selective H4R antagonists VUF10558 and JNJ-7777120 have been developed and investigated in vivo.^{10,11} It appears that [¹¹C]VUF10558 cannot cross the blood–brain barrier unlike the [¹¹C]JNJ-7777120; nevertheless, no relevant literature reporting the usefulness of [¹¹C]JNJ-7777120 has been published since its radiolabeling few years ago.¹² Moreover, the use of radiopharmaceuticals labeled with ¹¹C is limited by the short physical half-life of carbon-11 (20 min) and thus restricted to PET imaging departments closely linked to a cyclotron.

This constraint is avoided with the fluorine-18 radioisotope due to its relatively long half-life (110 min) and the possibility of generating fluorine-18 radiotracers, which can be shipped off-site. These main advantages led us to develop a fluorine-18 probe for PET imaging of H4R as a neuroinflammation target in order to improve the prospects for the understanding, early diagnosis, and treatment of brain diseases.¹¹

For this aim, we focused on a non-imidazole selective H4R antagonist series from which the JNJ-7777120 emerged (Figure 2). JNJ-7777120 was described to bind to the human H4R with high affinity (4.1 nM) and showed a greater than 1000-fold selectivity over the other histamine receptors.^{13,14} Interestingly the structure–activity relationship (SAR) described the fluorinated derivative **5** of JNJ-7777120, which showed a rather good inhibitory constant of 15 nM.¹⁴ We therefore decided to develop a radiolabeling procedure and prepared the [¹⁸F]**5** (Scheme 1), to evaluate its in vivo properties in a well-established rat model of excitotoxic neuroinflammation.^{15,16}

2 | EXPERIMENTAL

2.1 | General

¹H NMR and ¹³C NMR spectra were recorded on a Bruker DPX 250- or 400-MHz instrument using CDCl₃ or DMSO-*d*₆. The chemical shifts are reported in parts per million (δ scale), and all coupling constant (*J*) values are in Hertz (Hz). The following abbreviations were used to explain the multiplicities: s (singlet), d (doublet), t (triplet), q (quartet), m (multiplet), and dd (doublet of doublets). Melting points are uncorrected. IR absorption spectra were obtained on a PerkinElmer Paragon 1000 PC, and values are reported in cm⁻¹. HRMS was recorded on a Bruker maXis mass spectrometer. Monitoring of the reactions was performed using silica gel TLC plates (silica Merck 60 F₂₅₄). Spots were visualized by UV light at 254 and 356 nm. Column

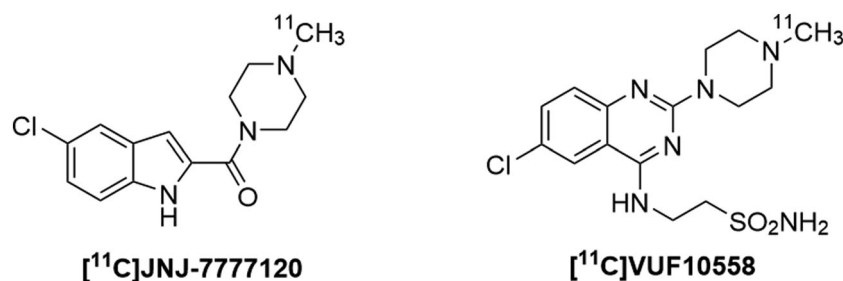


FIGURE 1 Tested carbon-11 H4R radiotracers

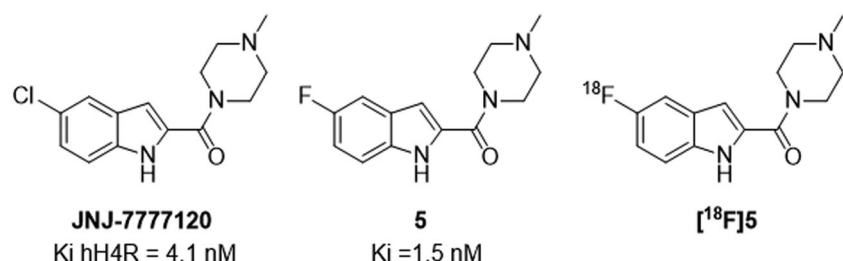
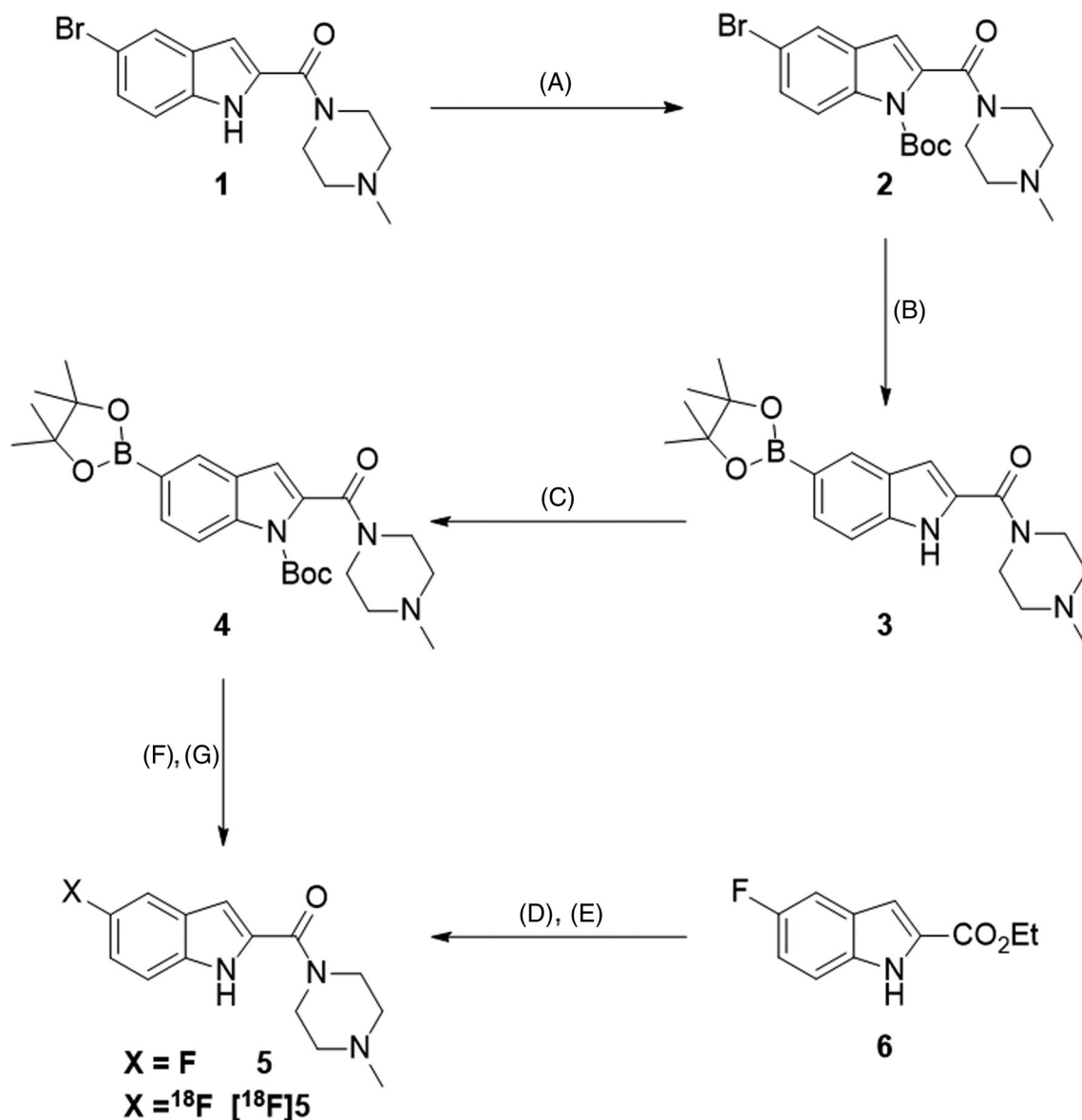


FIGURE 2 Structures of the 5-fluoro-1H-indol-2-yl(4-methyl-1-piperazinyl)methanone **5**, [¹⁸F]**5**, derived from the JNJ-7777120



SCHEME 1 Synthesis of the protected pinacol borane precursor **4**, the reference compound **5**, and the radiolabeling of [^{18}F]**5**. (A) Boc_2O (1.1 eq.), 4-DMAP (0.1 eq.), Et_3N (1.1 eq.), THF, r.t., 17 h, 99%. (B) B_2pin_2 (1.2 eq.), KOAc (0.3 eq.), $\text{Pd}(\text{dppf})\text{Cl}_2 \cdot \text{DCM}$ (0.04 eq.), 1,4-dioxane, 100°C , 17 h, 60%. (C) Boc_2O (1.1 eq.), 4-DMAP (0.1 eq.), Et_3N (1.1 eq.), THF, r.t., 12 h, 99%. (D) NaOH (10.8 eq.), EtOH, r.t., 48 h, then HCl 1 N, 90%. (E) SOCl_2 (6.7 eq.), 1-methylpiperazine (3.1 eq.), DCM, r.t., 1 h 30 min, 91%. (F) [^{18}F], $\text{K}_2\text{S}_2\text{O}_8$, DMF, pyridine, $\text{Cu}(\text{OTf})_2$, 120°C , 10 min. (G) Aqueous 3-N HCl solution, 100°C , 5 min

chromatographies were performed using silica gel 60 (0.063–0.200 mm, Merck). [^{18}F]Fluoride was produced using a PETtrace 10 cyclotron (GE Healthcare) via the classical $^{18}\text{O}(p,n)^{18}\text{F}$ reaction by bombardment of ^{18}O -enriched (98%) water with 16.5-MeV protons. Automated radiosyntheses for animal studies were performed in a sparsely modified TRACERlab Fx-FN Pro module (GE Medical Systems) including a semi-preparative HPLC equipped with UV and radiodetectors. The minor change made to the synthesizer consisted in connecting

valve VZ1 to a waste vial and not to the second reactor. A ZORBAX Eclipse XDB-C18 column (9.4×250 mm $5 \mu\text{m}$, Agilent) was used for semi-preparative purification with a wavelength at 254 nm for UV detection. HPLC quality controls were performed on an Ultimate 3000 system equipped with a UV detector and a radioactivity detector (PET metabolite, Bioscan). The analytical HPLC analyses were performed on an EVO column (150×4.6 mm, $2.6 \mu\text{m}$) at 291-nm wavelength and 1-ml/min flow.

2.2 | Chemistry

2.2.1 | *tert*-Butyl 5-bromo-2-(4-methylpiperazine-1-carbonyl)-1*H*-indole-1-carboxylate (**2**)

The solution of (5-bromo-1*H*-indol-2-yl)(4-methylpiperazin-1-yl)methanone (0.220 g, 0.70 mmol) in anhydrous THF (5 ml) was cooled down to 0°C under argon atmosphere. Et₃N (0.11 ml, 0.77 mmol, 1.1 eq.) and 4-DMAP (0.008 g, 0.07 mmol, 0.1 eq.) were added to the reaction mixture followed by Boc₂O (0.168 g, 0.77 mmol, 1.1 eq.). The reaction was allowed to warm up to r.t. and continued for 15 h. The mixture was then concentrated under vacuum, and the residue was purified by flash chromatography using DCM:MeOH (95:5) to afford the pure product as a pale brown oil (0.290 g, 99%). R_f = 0.28 (DCM:MeOH 95:5); IR (ATR diamond, cm⁻¹) ν 2978, 1739, 1635, 1478, 1434, 1350, 1336, 1250, 1234, 1201, 1141, 1093, 1075, 853; ¹H NMR (250 MHz, CDCl₃) δ 8.11–8.00 (m, 1H, H_{Ar}), 7.96 (s, 1H, H_{Ar}), 7.70 (dd, *J* = 8.4, 1.1 Hz, 1H, H_{Ar}), 6.52 (s, 1H, H_{Ar}), 3.79–3.61 (m, 2H, CH₂), 3.38–3.23 (m, 2H, CH₂), 2.49–2.34 (m, 2H, CH₂), 2.33–2.14 (m, 5H, CH₂ and N–CH₃), 1.26 (s, 9H, 3xCH₃); ¹³C NMR (63 MHz, CDCl₃) δ 163.0 (C=O), 148.7 (C=O), 137.7 (C_q), 132.3 (C_q), 131.5 (CH_{Ar}), 128.4 (CH_{Ar}), 128.0 (C_q), 114.6 (CH_{Ar}), 108.4 (CH_{Ar}), 84.7 (C_q), 54.4 (CH₂), 54.1 (CH₂), 53.3 (C_q), 46.6 (CH₂), 45.8 (N–CH₃), 41.5 (CH₂), 24.7 (3xCH₃); HRMS (EI-MS): calcd for C₁₉H₂₅BrN₃O₃ *m/z* 421.1001 [M + H]⁺, found 421.1008.

2.2.2 | (4-Methylpiperazin-1-yl)(5-(4,4,5,5-tetramethyl-1,3,2-dioxaborolan-2-yl)-1*H*-indol-2-yl)methanone (**3**)

The solution of **2** (0.2 g, 0.47 mmol), (Bpin)₂ (0.142 g, 0.56 mmol, 1.2 eq.), and KOAc (0.138 g, 1.41 mmol, 3.0 eq.) in 1,4-dioxane (3 ml) was flushed with argon for 15 min. Pd(dppf)Cl₂·DCM (0.015 g, 0.02 mmol, 8.0 mol%) was added to the solution, and the reaction mixture was sealed in a tube and heated up to 130°C for 17 h. The resulting solution was filtered through a pad of Celite[®] and concentrated under reduced pressure. The crude product was purified by flash chromatography using DCM:MeOH (95:5) as an eluent resulting in the desired product as a beige solid (0.101 g, 60%). R_f = 0.33 (DCM:MeOH 95:5); mp 220–222°C; IR (ATR diamond, cm⁻¹) ν 3265, 2786, 1595, 1572, 1478, 1442, 1380, 1355, 1327, 1287, 1254, 1205, 1141, 750; ¹H NMR (250 MHz, DMSO-*d*₆) δ 11.48 (s, 1H, NH), 8.02 (s, 1H, H_{Ar}), 7.50 (d, *J* = 8.3 Hz, 1H, H_{Ar}), 7.42 (d, *J* = 8.3 Hz, 1H, H_{Ar}), 6.79 (s, 1H, H_{Ar}), 3.74 (t, 4H, 2xCH₂), 2.39 (t, 4H, 2xCH₂),

2.24 (s, 3H, N–CH₃), 1.32 (s, 12H, 4xCH₃); ¹³C NMR 80°C (63 MHz, DMSO-*d*₆) δ 161.7 (C=O), 137.6 (C_q), 130.1 (CH_{Ar}), 128.8 (CH_{Ar}), 128.3 (C_q), 126.4 (C_q), 111.1 (CH_{Ar}), 103.9 (CH_{Ar}), 83.8 (2xC_q), 54.3 (2xCH₂), 45.2 (N–CH₃), 44.1 (2xCH₂), 24.4 (4xCH₃); HRMS (EI-MS): calcd for C₂₀H₂₉BN₃O₃ *m/z* 370.2297 [M + H]⁺, found 370.2301.

2.2.3 | *tert*-Butyl 2-(4-methylpiperazine-1-carbonyl)-5-(4,4,5,5-tetramethyl-1,3,2-dioxaborolan-2-yl)-1*H*-indole-1-carboxylate (**4**)

The solution of **3** (0.104 g, 0.3 mmol) in anhydrous THF (5 ml) was cooled down to 0°C under argon atmosphere. Et₃N (0.08 ml, 0.6 mmol, 1.1 eq.) and 4-DMAP (0.004 g, 0.03 mmol, 0.1 eq.) were added to the reaction mixture followed by Boc₂O (0.072 g, 0.33 mmol, 1.1 eq.). The reaction was allowed to warm up to r.t. and continued for 12 h. The mixture was then concentrated under vacuum, and the residue was purified by flash chromatography using DCM:MeOH (95:5) to afford the pure product as a yellow oil (0.075 g, 59%). R_f = 0.51 (DCM:MeOH 95:5); IR (ATR diamond, cm⁻¹) ν 2978, 1738, 1644, 1434, 1350, 1336, 1292, 1251, 1233, 1162, 1141, 1092, 1074, 1001, 853, 729; ¹H NMR (400 MHz, CDCl₃) δ 8.13 (d, *J* = 8.4 Hz, 1H), 8.03 (s, 1H), 7.78 (d, *J* = 8.4 Hz, 1H), 6.60 (s, 1H), 3.78 (t, *J* = 9.1 Hz, 2H, CH₂), 3.41–3.34 (m, 2H, CH₂), 2.49 (t, *J* = 4.9 Hz, 2H, CH₂), 2.36–2.31 (m, 5H), 1.61 (s, 9H, 3xCH₃), 1.35 (s, 12H, 4xCH₃); ¹³C NMR (63 MHz, CDCl₃) δ 163.3 (C=O), 149.0 (C=O), 138.0 (C_q), 132.7 (C_q), 131.7 (CH_{Ar}), 128.7 (CH_{Ar}), 128.3 (C_q), 114.9 (CH_{Ar}), 108.7 (CH_{Ar}), 85.0 (C_q), 83.9 (2xC_q), 54.8 (CH₂), 54.5 (CH₂), 46.9 (CH₂), 46.6 (N–CH₃), 41.8 (CH₂), 28.2 (3xCH₃), 25.0 (4xCH₃); HRMS (EI-MS): calcd for C₂₅H₃₇BN₃O₅ *m/z* 470.2821 [M + H]⁺, found 470.2823.

2.2.4 | (5-Fluoro-1*H*-indol-2-yl)(4-methyl-1-piperazinyl)methanone (**5**)

The commercially available compound **6** (0.607 g, 2.93 mmol), NaOH (1.27 g, 31.78 mmol), and ethanol (20 ml) were mixed at r.t. for 48 h. The mixture was then concentrated under vacuum, and the residue was adjusted to pH 1 with HCl 1 N. EtOAc (20 ml) was added, and the organic layer was extracted, washed with water (10 ml), dried over MgSO₄, filtered, and concentrated under vacuum. The crude mixture was dissolved in DCM (20 ml), and SOCl₂ (1.28 ml, 3.1 eq.) was slowly added. The mixture was stirred at r.t. for 1 h, and

the amine (0.87 ml, 3.1 eq.) was added. The solution was stirred at r.t. for 1 h 30 min and then concentrated under vacuum. EtOAc (20 ml) was added, and the solution was adjusted to pH 9 with NaOH 1 N. The organic phase was extracted, washed with water (10 ml), dried over MgSO₄, filtered, and concentrated under vacuum to afford the pure product as a yellow solid (0.627 g, 82%). ¹H NMR (250 MHz, DMSO-*d*₆): δ 11.71 (s, NH), 7.39 (m, 2H, H_{Ar}), 7.05 (m, 1H, H_{Ar}), 6.80 (m, 1H, H_{Ar}), 3.93–3.74 (br, 4H, 2xCH₂), 2.68 (m, 4H, 2xCH₂), 2.42 (s, 3H, CH₃). The physical data are in accordance with the literature.¹⁴

2.3 | Radiochemistry

2.3.1 | 5-[¹⁸F]-Fluoro-1*H*-indol-2-yl) (4-methyl-1-piperazinyl)methanone (**5**)

Prior to the automation on the TRACERlab FX-FN Pro (GE) synthesizer, attempts in warm conditions were performed to optimize temperature and reaction time reaction based on a similar previous approach.¹⁷ The optimized conditions defined during this development phase were applied for the production on the synthesizer. As previously reported,¹⁸ [¹⁸F]fluoride ion was produced on a cyclotron (PET trace, GE Healthcare) by irradiation of enriched ¹⁸O H₂O with protons via the ¹⁸O(*p,n*)¹⁸F nuclear reaction. [¹⁸F]fluoride was transferred to a

modified TRACERlab FX-FN Pro (GE) synthesizer and passed through an anion-exchange resin (Waters, Sep-Pak Accell Light QMA cartridge in the carbonate form). Using a boronic ester to afford the nucleophilic aromatic substitution, the trapped [¹⁸F]fluoride was released from the cartridge with the Mossine et al.¹⁹ eluent solution consisting of 550 μl of aqueous solution containing 5 mg of potassium trifluoromethanesulfonate and 50 μg of potassium in water. Azeotropic distillation was performed twice using each time 1 ml of acetonitrile at 100°C under He flow and vacuum. To the anhydrous [¹⁸F]KF solution, precursor **4** (2.0 mg), Cu(OTf)₂ (3.5 mg), and pyridine (40 μl) were added and dissolved in DMF (960 μl). Then, the mixture was heated at 120°C for 10 min and cooled to 100°C to perform hydrolysis with an aqueous 3-N HCl solution (1 ml) for 5 min. The solution was cooled to 40°C and neutralized with an aqueous 0.5-M NaOH solution (7 ml). The crude solution was passed through a *t*-C18 Sep-Pak Plus cartridge (Waters). The reactor and cartridge were rinsed with water (5 ml), and the crude compound was eluted from the cartridge with acetonitrile (1 ml). Prior to HPLC purification, the crude solution was diluted with 2 ml of the mobile phase (acetonitrile/(ammonium acetate, 0.1 M + 0.2% Et₃N) 25/75. Purification occurred on a ZORBAX Eclipse XDB-C18 (9.4 × 250 mm, 5 μm, Agilent) at a 4 ml/min flow (Figure 3). The collected peak was then diluted in water (20 ml), and the solution was trapped on

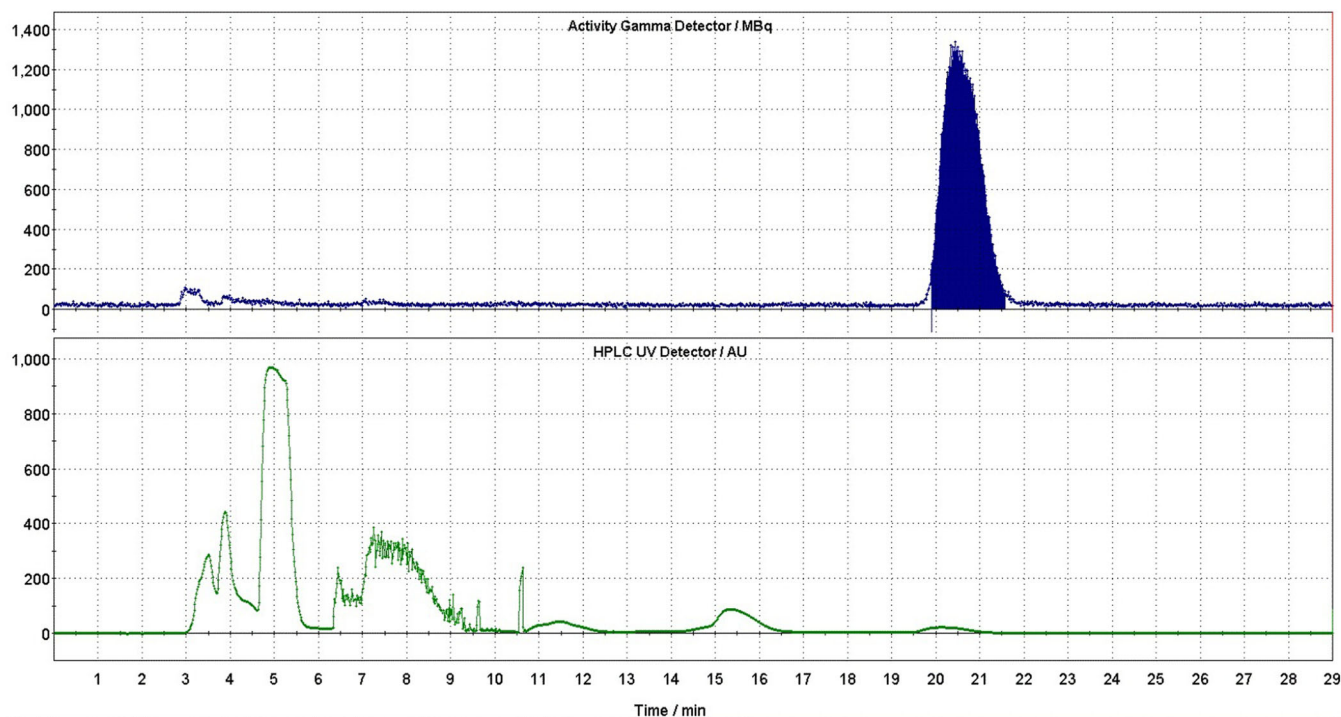


FIGURE 3 Semi-preparative purification of [¹⁸F]**5** on a ZORBAX Eclipse XDB-C18 (5 μm, 9.4 × 250 mm) with a 4-ml/min flow using acetonitrile/(ammonium acetate 0.1 M + 0.2% Et₃N): 25/75 as mobile phase. Top, radioactivity signal; bottom, UV signal

a *t*C18 cartridge (Waters Sep-Pak Accell Light *t*C18 cartridge). The cartridge was rinsed with water (5 ml), and [^{18}F]**5** was eluted from the *t*C18 with EtOH (0.5 ml). The formulation was completed by adding 0.9% NaCl solution (4.5 ml).

2.4 | Quality control and stability

The chemical and radiochemical purity of the final product for clinical use was determined by HPLC analysis using a Kinetex EVO column (4.6 × 150 mm, 2.6 μm, Phenomenex, USA) and eluted with acetonitrile/(ammonium acetate, 0.1 M + 0.2% Et₃N) 30/70 at a flow rate of 1.0 ml/min (Figure 4). The stability of the injectable solution was checked by HPLC up to 4 h after the end of preparation. To operate this control, 100 μl of the radiotracer solution was mixed with 1 ml of rat plasma and incubated at 37°C. Then,

500 μl of acetonitrile were added, the organic layer was removed and filtered, 20 μl was loaded onto the HPLC, and the stability was checked at 4-h time point after production.

2.5 | Biological studies

2.5.1 | In vitro experiments

The affinity of **5** towards H4R was determined by CEREP (Le Bois l'Eveque, 86600 Celle-Lévescault, France) according to their standard assay protocols, using HEK-293 cells expressing the human recombinant H4R and [^3H]histamine as a reference tracer (see <http://www.cerep.fr/cerep/users/pages/catalog/search/catalog.asp>). For the biological experiments, only one production of [^{18}F]**5** was used with a molar activity of 132.64 GBq/μmol.

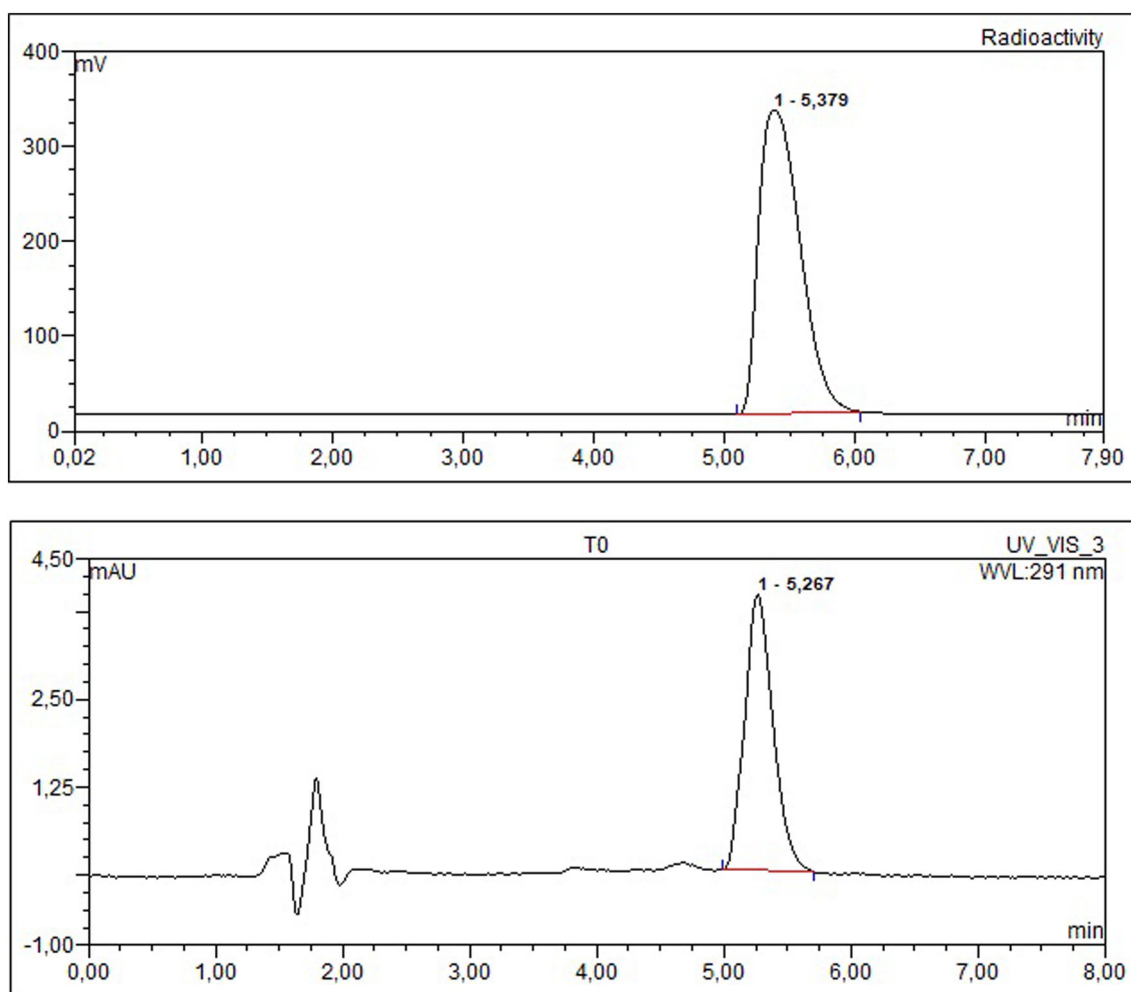


FIGURE 4 Analytical HPLC chromatogram of the final product [^{18}F]**5** after HPLC purification. Chromatograms were obtained on a Kinetex EVO C18 (2.6 μm, 4.6 × 150 mm). HPLC was operated in isocratic mode at 1-ml/min flow rate using acetonitrile/(ammonium acetate 0.1 M + 0.2% Et₃N): 30/70 as mobile phase

2.5.2 | In vivo experiments

A total of 14 male adult Wistar rats were included (CERJ, Le Genest-Saint-Isle, France). Animals were bred, and experiments were conducted according to the European Community Council Directive 2010/63/EU for laboratory animal care and French rules (Authorization No. 2015022011523044). All rats were subjected to a stereotaxic injection of quinolinic acid (150 nmol; Sigma-Aldrich, Lyon, France) in the right striatum using a previously described procedure.²⁰ At 7 days after lesion, they were randomly divided into two groups of six animals, that is, the control and JNJ groups. The latter received an intravenous injection of the H4R-specific antagonist JNJ-7777120 (3 mg/kg; Tocris, R&D Systems Europe, Lille, France) 15 min before the tracer injection. Animals of both groups were then intravenously injected with [¹⁸F]5 (2–5 MBq in 0.15 ml of saline) and sacrificed 1 h after injection. The blood, brain regions, and peripheral tissue samples were then removed and weighed, and their radioactivity was measured using a γ -counter (2480 Gamma counter Wizard, PerkinElmer, France). The percentage of injected dose per gram of tissue (%ID/g) was calculated by comparison with samples of the injected solution.

2.5.3 | μ PET imaging

In parallel, two rats were intravenously injected with [¹⁸F]5 (47 MBq), and their brains were scanned with a μ PET/CT system (SuperArgus, Sedecal, Madrid, Spain) during 120 min under continuous gas anesthesia (isoflurane, Baxter, France), according to a previously described procedure.¹⁸ The time-activity curve was expressed as the average of % injected dose/g measured in the whole brain of both animals.

3 | RESULTS AND DISCUSSION

3.1 | Chemistry

The synthesis of precursor **4** for the radiosynthesis and the reference compound **5** is depicted in Scheme 1. The synthesis of bromo derivative **1** was achieved in high yield according to the reported amidification procedure, which involved 5-bromo-1*H*-indole-2-carboxylic acid and *N*-methyl-piperazine in the presence of carbonyldiimidazole. As the purpose was to determine the potency of the tracer candidate to target the H4R, and the radiochemical (RCY) was not the primary objective, we initially planned a one-step radiosynthesis strategy

using the unprotected indole, but assays of boronylation of **1** failed. We therefore protected the indolic nitrogen atom by a *t*-Boc group in a nearly quantitative manner, and derivative **2** was subjected to the expected palladium catalyzed boronylation. Optimized conditions involved the use of bis(pinacolato)diborane, Pd(dppf)Cl₂·DCM, as catalyst in the presence of KOAc as base in dioxane at 100°C for 17 h. However, despite efforts, the *t*-Boc group did not survive the high temperature reaction and long reaction time. Purification led directly to the pure deprotected derivative **3** in 60% yield. A further protection of the indolic nitrogen atom was performed using a slight excess of Boc₂O in basic media to afford **4** in a satisfying yield. The reference compound **5** was obtained from the commercially ethyl 5-fluoroindole-2-carboxylate **6** in two steps. The first one consisted in a saponification with NaOH, to afford the corresponding carboxylic acid. Then, the crude carboxylic acid is transformed into its corresponding acyl chloride via thionyl chloride followed by amidation with *N*-methylpiperazine. Compound **5** was obtained in 82% overall yield.

3.2 | Radiochemistry

To radiolabel compound **5** with [¹⁸F]fluoride, we adopted a two-step procedure, that is, fluorination from a pinacol borane entity followed by acidic deprotection of the indole (Scheme 1). As previously reported^{19,21} and based on previous experiments,¹⁷ we achieved fluorination using an eluent solution containing the fluorine-18 from QMA and KOTf and K₂CO₃ in CH₃CN/water. To this medium was added a solution containing the precursor, Cu(OTf)₂, a low amount of pyridine and the whole dissolved in DMF. The condition of the first step was optimized by a warm approach as already performed by our team for a COX-2 tracer.¹⁷ The first experiments conducted at 100°C for 5 min did not enable the incorporation of fluorine-18 onto precursor **4**. A longer reaction time of 20 min resulted in 16.5% incorporation. To increase the radiochemical yield, we also increased the reaction temperature up to 130°C. Incorporation yields at 120°C and 130°C gave similar results of 28% and 30%, respectively. Nevertheless, at 130°C, we observed that an additional radioactive peak appeared and moreover that a prolonged reaction time resulted in a decrease in incorporation yield, an increase of the side-product radioactive peak, and a degradation of the precursor. Then, the optimized conditions were applied on the synthesizer as follow with a fluorination step performed at 120°C during 10 min immediately followed by the hydrolysis at 100°C for 5 min using a 3-N HCl aqueous solution. The non-optimized production afforded [¹⁸F]5

in a $5.7 \pm 1.35\%$ radiochemical yield, in 78 min with a molar activity of 100.7 ± 34.5 GBq/ μmol ($n = 3$). In comparison to results obtained with the COX-2 tracer,¹⁷ we observed that the preparation of [^{18}F]5 resulted in much lower yields in warm conditions (30% vs. 92%) as with the synthesizer (5.7% vs. 49%). The differences in RCY could be due to a hydrolysis of the Boc group by [^{18}F] fluoride ions making the nucleophilic substitution less conducive and entering directly in competition with the desired reaction.²² The radiochemical stability was checked up to 4 h after production without observing degradation of the radiotracer, and radiochemical purity remained greater than 99%. The stability of [^{18}F]5 in rat plasma at 37°C was checked up to 4 h, and no degradation of the radiotracer was observed.

3.3 | Biological studies

We observed that compound 5 displayed a K_i of 1.5 nM in the condition tested by the CEREP for human H4R. This affinity was in agreement with the previously published data¹⁴ and in the same range as the affinity obtained for the first described H4R antagonist, that is, JNJ-777120, which is the chlorinated analog of 5,¹³ and also for A-987306, which has a different chemical structure.²³

These literature data also highlighted that these affinities were quite similar between human and rodent H4 receptors, although species differences in these receptors have been described.^{24,25} In addition, although contradictory data have been found, an extensive analysis of them indicated that the presence of H4R on neurons is unlikely, whereas its specific expression by microglia is recognized.^{3,26,27} Indeed, if the presence of H4 mRNA is recognized, the expression of protein is still questionable due to the lack of specificity of the available antibodies.²⁸ In this context, we evaluated the in vivo binding of our new tracer in a well-known rat model of microglial activation.¹⁵

As illustrated, we observed that [^{18}F]5 entered the rat brain just after intravenous injection, with a peak around 5 min after injection and then a progressive decrease followed by a low level from 30 min after injection. As the recorded activity was homogeneous across the whole brain, it is represented as a single curve (Figure 5).

As reported in Table 1, the uptake of [^{18}F]5 1 h after injection was homogeneous in different regions and was similar in both sides of the brain, despite the microglial activation we induced in the right side.¹⁵ In addition, the preinjection of a saturating dose of the H4R antagonist JNJ-777120 did not induce any modification in the tracer accumulation, both in central and in peripheral tissues (Tables 1 and 2).

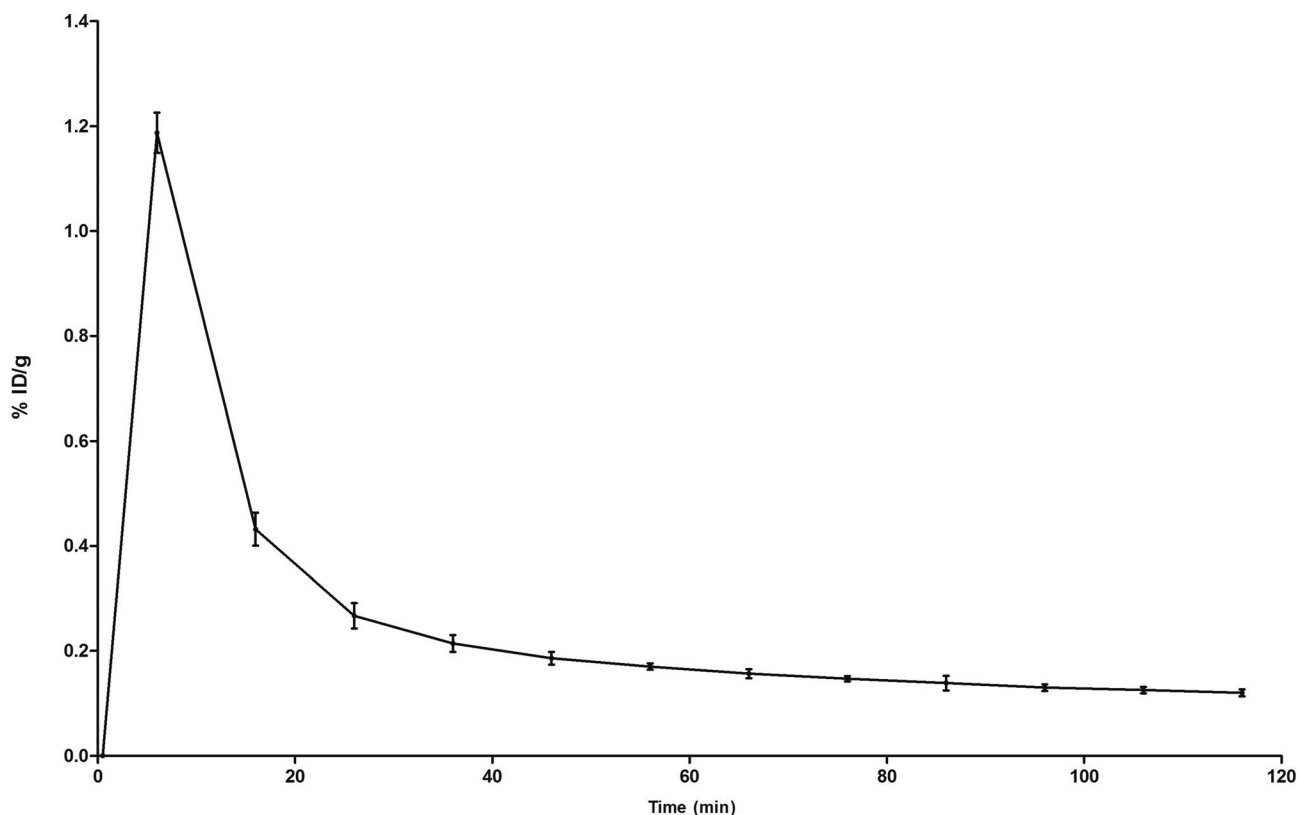


FIGURE 5 Time-activity curve of [^{18}F]5 in the rat whole brain. Mean \pm SEM; $n = 2$

TABLE 1 Rat brain biodistribution of [¹⁸F]5

	Right Cx	Left Cx	Right Stri	Left Stri	Right Hippoc	Left Hippoc	Cereb
Control group	0.10 ± 0.01	0.10 ± 0.01	0.15 ± 0.02	0.14 ± 0.02	0.16 ± 0.02	0.16 ± 0.02	0.12 ± 0.01
JNJ group	0.13 ± 0.02	0.13 ± 0.02	0.18 ± 0.04	0.17 ± 0.02	0.18 ± 0.03	0.18 ± 0.02	0.14 ± 0.03

Note: Results are expressed as mean % of injected dose/g tissue ± SD; *n* = 6 per group. All animals received an injection of QA in the right striatum 7 days before the biodistribution experiment. Rats from the JNJ group received an intravenous injection of JNJ-7777120 (3 mg/kg) 15 min before the tracer injection. All animals were sacrificed 1 h after [¹⁸F]5 injection.

Abbreviations: Cereb, cerebellum; Cx, cortex; Hippoc, hippocampus; Stri, striatum.

TABLE 2 Rat biodistribution of [¹⁸F]5 in peripheral tissue

	Bl	He	Lu	Liv	Sp	Kid	Int	Mus	Bo
Control group	0.11 ± 0.01	0.10 ± 0.02	0.31 ± 0.06	0.96 ± 0.14	0.15 ± 0.01	0.73 ± 0.13	0.10 ± 0.07	0.07 ± 0.01	0.10 ± 0.01
JNJ group	0.11 ± 0.02	0.11 ± 0.02	0.35 ± 0.15	0.89 ± 0.24	0.20 ± 0.03	0.67 ± 0.13	0.12 ± 0.02	0.09 ± 0.04	0.11 ± 0.02

Note: Results are expressed as mean of % injected dose/g tissue ± SD; *n* = 6 per group. Rats from the JNJ group received an intravenous injection of JNJ-7777120 (3 mg/kg) 15 min before the tracer injection. All animals were sacrificed 1 h after [¹⁸F]5 injection.

Abbreviations: Bl, blood; Bo, bone; He, heart; Int, intestine; Kid, kidney; Liv, liver; Lu, lung; Mus, muscle; Sp, spleen.

To our knowledge, no useful PET tracer is to date available for H4R.¹¹ The present study shows that, despite a nanomolar affinity for the target and appropriate molar activity, the fluorinated derivative of JNJ-7777120, that is, [¹⁸F]5, did not colocalize with the brain activated microglia expressed in the rat model of acute neuroinflammation that we used. This could be linked to an in vivo nonspecific binding of the tracer to H4R and/or to a low expression of this receptor in this model. In any case, this highlights the need to develop new chemical structures as ligands for this promising target.

4 | CONCLUSION

We successfully prepared the fluorinated derivative of JNJ-7777120, compound **5**, and performed in vitro evaluation, radiolabeling, and biological characterization of the tracer. The in vitro evaluation of **5** gave a *K_i* value of 1.5 nM, high enough to perform its radiolabeling with fluorine-18 and complete the biological evaluation. Radiolabeling of **5** was achieved in a two-step procedure, with a low non-optimized radiochemical yield of 5.7 ± 1.37% but in sufficient amount of radioactivity to perform biodistribution and μPET imaging in rats. Unfortunately, while [¹⁸F]5 appears able to cross the blood–brain barrier, we observed that its brain accumulation seems not reflecting the distribution of H4R, in particular by activated microglia.

ACKNOWLEDGEMENT

This research was supported by grants from the Labex IRON [ANR-11-LABX-0018-01] and InMIND program which are associated to this work.

ORCID

Sylvie Chalon  <https://orcid.org/0000-0003-1865-8380>

Sylvain Routier  <https://orcid.org/0000-0002-2823-0591>

Frédéric Buron  <https://orcid.org/0000-0001-5773-1515>

Johnny Vercouillie  <https://orcid.org/0000-0002-7474-7778>

REFERENCES

- Haas HK, Sergeeva OA, Selbach O. Histamine in the nervous system. *Physiol Rev*. 2008;88(3):1183-1241. <https://doi.org/10.1152/physrev.00043.2007>
- Neumann D, Schneider EH, Seifert R. Analysis of histamine receptor knockout mice in models of inflammation. *J Pharmacol Exp Ther*. 2014;348(1):2-11. <https://doi.org/10.1124/jpet.113.204214>
- Schneider EH, Seifert R. The histamine H4-receptor and the central and peripheral nervous system: a critical analysis of the literature. *Neuropharmacology*. 2016;106:116-128. <https://doi.org/10.1016/j.neuropharm.2015.05.004>
- Frick L, Rapanelli M, Abbasi E, Ohtsu H, Pittenger C. Histamine regulation of microglia: gene-environment interaction in the regulation of central nervous system inflammation. *Brain Behav Immun*. 2016;57:326-337. <https://doi.org/10.1016/j.bbi.2016.07.002>
- Seifert R, Schneider EH, Dove S, et al. Paradoxical stimulatory effects of the “standard” histamine H4-receptor antagonist JNJ7777120: the H4 receptor joins the club of 7 transmembrane domain receptors exhibiting functional selectivity. *Mol Pharmacol*. 2011;79(4):631-638. <https://doi.org/10.1124/mol.111.071266>
- Zhou P, Homberg JR, Fang Q, et al. Histamine-4 receptor antagonist JNJ777120 inhibits pro-inflammatory microglia and prevents the progression of Parkinson-like pathology and behaviour in a rat model. *Brain Behav Immun*. 2019;76:61-73. <https://doi.org/10.1016/j.bbi.2018.11.006>
- Glass CK, Saijo K, Winner B, Marchetto MC, Gage FH. Mechanisms underlying inflammation in neurodegeneration. *Cell*. 2010;140(6):918-934. <https://doi.org/10.1016/j.cell.2010.02.016>

8. Jacobs AH, Tavitian B, INMiND Consortium. Noninvasive molecular imaging of neuroinflammation. *J Cereb Blood Flow Metab.* 2012;32(7):1393-1415. <https://doi.org/10.1038/jcbfm.2012.53>
9. Tronel C, Largeau B, Santiago Ribeiro MJ, Guilloteau D, Dupont AC, Arlicot N. Molecular targets for PET imaging of activated microglia: the current situation and future expectations. *Int J Mol Sci.* 2017;18(4):802-823. <https://doi.org/10.3390/ijms18040802>
10. Janssen B, Vugts DJ, Funke U, et al. Imaging of neuroinflammation in Alzheimer's disease, multiple sclerosis and stroke: recent developments in positron emission tomography. *Biochim Biophys Acta.* 2016;1862(3):425-441. <https://doi.org/10.1016/j.bbadis.2015>
11. Funke U, Vugts D, Janssen B, et al. ¹¹C-labeled and ¹⁸F-labeled ligands for subtype-specific imaging of histamine receptors in the brain. *J Label Compd Radiopharm.* 2013;56(3-4):120-129.
12. Leurs R, Smits R, Mooijer M, de Esch I, Windhorst B. Synthesis and in-vivo evaluation of human histamine H₄ receptor modulators [¹¹C]JNJ7777120 and [¹¹C]VUF10558 for monitoring inflammatory. EHRS XXXVIIth Annual Meeting, 2008; 26, 87.
13. Thurmond RL, Desai PJ, Dunford PJ, et al. A potent and selective histamine H₄ receptor antagonist with anti-inflammatory properties. *J Pharmacol Exp Ther.* 2004;309(1):404-413.
14. Jablonowski JA, Grice CA, Chai W, et al. The first potent and selective non-imidazole human histamine H₄ receptor antagonists. *J Med Chem.* 2003;46(19):3957-3960.
15. Arlicot N, Tronel C, Bodard S, et al. Translocator protein (18 kDa) mapping with [¹²⁵I]-CLINDE in the quinolinic acid rat model of excitotoxicity: a longitudinal comparison with microglial activation, astrogliosis, and neuronal death. *Mol Imaging.* 2014;13:4-11.
16. Arlicot N, Katsifis A, Garreau L, et al. Evaluation of CLINDE as potent translocator protein (18 kDa) SPECT radiotracer reflecting the degree of neuroinflammation in a rat model of microglial activation. *Eur J Nucl Med Mol Imaging.* 2008; 35(12):2203-2211. <https://doi.org/10.1007/s00259-008-0834-x>
17. Elie J, Vercouillie J, Arlicot N, et al. Design of selective COX-2 inhibitors in the (aza)indazole series. Chemistry, in vitro studies, radiochemistry and evaluations in rats of a [¹⁸F] PET tracer. *J Enzyme Inhib Med Chem.* 2019;34(1):1-7.
18. Ouach A, Vercouillie J, Bertrand E, et al. Bis(het)aryl-1,2,3-triazole quinuclidines as α 7 nicotinic acetylcholine receptor ligands: synthesis, structure affinity relationships, agonism activity, [¹⁸F]-radiolabeling and PET study in rats. *Eur J Med Chem.* 2019;179:449-469.
19. Mossine AV, Brooks AF, Makaravage KJ, et al. Synthesis of [¹⁸F]arenes via the copper-mediated [¹⁸F]fluorination of boronic acids. *Org Lett.* 2015;17(23):5780-5783. <https://doi.org/10.1021/acs.orglett.5b02875>
20. Foucault-Fruchard L, Doméné A, Page G, et al. Neuroprotective effect of the alpha 7 nicotinic receptor agonist PHA 543613 in an in-vivo excitotoxic adult rat model. *Neuroscience.* 2017;356:52-63.
21. Tredwell M, Preshlock SM, Taylor NJ, et al. A general copper-mediated nucleophilic ¹⁸F fluorination of arenes. *Angew Chem Int Ed.* 2014;53(30):7751-7755. <https://doi.org/10.1002/anie.201404436>
22. Jacquemard U, Bénéteau V, Lefoix M, Routier S, Mérou JY, Coudert G. Mild and selective deprotection of carbamates with Bu₄NF. *Tetrahedron.* 2004;60(44):10039-10047.
23. Liu H, Altenbach RJ, Carr TL, Chandran P, Hsieh GC, et al. cis-4-(Piperazin-1-yl)-5,6,7a,8,9,10,11,11a-octahydrobenzofuro [2,3-*h*]quinazolin-2-amine (A-987306), a new histamine H₄R antagonist that blocks pain responses against carrageenan-induced hyperalgesia. *J Med Chem.* 2008;51:7094-7098.
24. Lim HD, de Graaf C, Jiang W, et al. Molecular determinants of ligand binding to H₄R species variants. *Mol Pharmacol.* 2010;77(5):734-743. <https://doi.org/10.1124/mol.109.063040>
25. Nijmeijer S, de Graaf C, Leurs R, Vischer HF. Molecular pharmacology of histamine H₄ receptors. *Front Biosci.* 2012;17: 2089-2106. <https://doi.org/10.2741/4039>
26. Ferreira R, Santos T, Gonçalves J, et al. Histamine modulates microglia function. *J Neuroinflammation.* 2012;9(1):90-105.
27. Strakhova MI, Nikkel AL, Manelli AM, et al. Localization of histamine H₄ receptors in the central nervous system of human and rat. *Brain Res.* 2009;1250:41-48.
28. Beerman S, Seifert R, Neumann D. Commercially available antibodies against human and murine histamine H₄-receptor lack specificity. *Naunyn Schmiedeberg's Arch Pharmacol.* 2012; 385(2):125-135.

How to cite this article: Zak A, Lemaire L, Chalon S, et al. [¹⁸F]-labeled positron emission tomography ligand for the histamine H₄ receptor. *J Label Compd Radiopharm.* 2021;1-10. <https://doi.org/10.1002/jlcr.3929>